Clock and Carrier Synchronized Multi-Band Wireless Communications Enabled by Frequency Comb Dissemination in Radio Access Networks

Zichuan Zhou, *Student Member, IEEE,* Dhecha Nopchinda, *Member, IEEE,* Izzat Darwazeh, *Senior Member, IEEE,* and Zhixin Liu, *Senior Member, IEEE*

***Abstract*—Next generation radio access network requires multi-band wireless communication between the distributed unit (DU) and the radio unit (RU) to maximize millimeter wave spectrum usage and thus improving data capacity. Besides, the increasing demand of high accuracy positioning and low latency applications such as self-driving car motivates the need for low timing jitter synchronous clock distribution in future radio access network. One of the key enabling technologies for such a system is using an optical frequency comb to distribute low phase noise and synchronous clock and RF carriers, which can 1) support simultaneous multi-band wireless communication and 2) enable clock synchronisation between DUs and RUs. We propose using optical frequency comb to achieve simultaneous synchronised clock and RF carrier distribution. In this proof-of-concept experiment, a frequency synchronised multi-band 16QAM wireless transmission at 12.5, 25 and 37.5GHz has been demonstrated, covering Ku, K and Ka bands at the same time. The optical frequency comb is distributed from the DU to the RU through a standard single mode fiber (SSMF) and a broadband photodetector generates the RF frequency comb through photomixing. We have demonstrated low phase noise RF carrier distribution over 22km SSMF transmission with 70fs root-mean-squared (rms) jitter. The low rms jitter enables high order modulation format and the ability of maintaining jitter performance after SSMF transmission validates the system scalability. Additionally, we analytically modeled the impact of the fiber chromatic dispersion on RF carrier power generated using the proposed scheme. Based on this model we have demonstrated a novel optical spectrum shaping technique to eliminate power fading of RF frequency comb after transmission. Finally, the impact of the fiber chromatic dispersion and the comb seed laser phase noise on the distributed RF carrier phase noise are experimentally investigated, providing benchmark for optical frequency comb design.**

***Index Terms*—Radio Access Network, Optical Frequency Comb, mm-wave Transmission, Clock Synchronization**

I. Introduction

THE rise of beyond 100 Gb/s wireless links and latency sensitive applications such as virtual reality, connected car fleets, holography streaming on-demand has stimulated broadband and low latency wireless signal transmission, in the front-haul, between distributed units (DU) and radio units (RU) [1], [2], [3], [4]. Existing radio access network predominately utilizes sub-6GHz frequency band for mobile cellular network. Since sub-6GHz frequency bands becomes highly congested, wireless transmission at frequency bands beyond 6GHz becomes a key aspect for next generation 5G and 6G wireless data communication [1], [3], [5]. Moreover, simultaneously transmitting over multiple frequency bands is being considered in future radio access networks to enable flexible access to any available frequency bands for high aggregated capacity [6]. Further, future time-sensitive wireless applications, such as autonomous vehicles, drone swarm, AR/VR, WLAN and wireless sensor networks require sub-nanosecond timing precision, highlighting the need for precise clock synchronization amongst users [7], [8], [9], [10], [11], [12].

One key challenge of wireless transmission beyond 6GHz is the high propagation loss of wireless signal over air. To address this, Radio-over-fiber (RoF) technology has been developed. By transmitting wireless signal over optical fiber instead of over air, the wireless signal can be distributed over tens of kilometers, enhancing the coverage. RoF can be further classified into Radio frequency-over-fiber (RFoF) and baseband-over-fiber (BBoF). In RFoF, a broadband digital-to-analog convertor (DAC) is used to generate wireless signal at desired carrier frequency [13], [14], which is then converted into optical domain and distributed to RU through optical fiber. A broadband photodetector at RU side outputs the beat tone between optical carrier and modulation signal, which corresponds to the RF signal centered at desired carrier frequency for wireless transmission. One key limitation of this approach is that multiple broadband ADCs, DACs, photodectors and modulators are required to cover multiple frequency bands, which significantly increases cost and complexity. Another limitation of this approach is the RF power fading induced by optical fiber chromatic dispersion [13]. Although single sideband modulation can eliminate power fading, this leads to increased cost and complexity [15].

On the other hand, in BBoF system, a low bandwidth DAC is used to generate baseband wireless signal, which is then converted to optical domain and transmitted through optical fiber and arrives at RU. At RU side, a RF mixer mixes received baseband signal with RF carrier at desired frequency to generate wireless signal. As the baseband signal bandwidth is low, BBoF features higher tolerance to fiber chromatic dispersion [16], [17], [18]. Moreover, as only low bandwidth optoelectronic components are required, BBoF permits

Manuscript received xx xx, 2023. The authors acknowledge EPSRC ORBITS (EP/V051377/1) and EPSRC TRACCS (EP/W026252/1) for the funding support. Dr. D. Nopchinda was funded by the Leverhulme Trust.

Z. Zhou, I. Darwazeh and Z. Liu are with the Department of Electronic and Electrical Engineering, University College London, Gower Street, London WC1E 6BT, U.K. (e-mail: zczlzz0@ucl.ac.uk; i.darwazeh@ucl.ac.uk; zhixin.liu@ucl.ac.uk). D. Nopchinda is with Gotmic AB, 411 33 Gothenburg, Sweden (e-mail: dhecha@ieee.org).

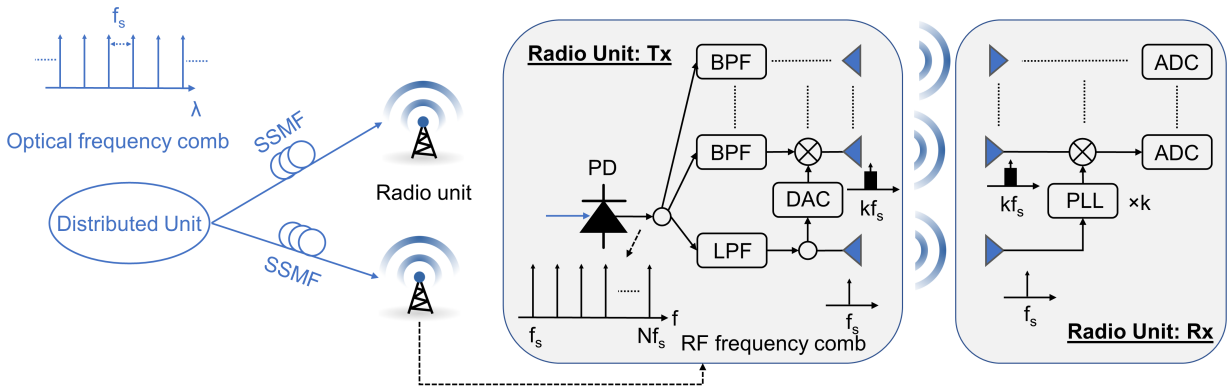

Fig. 1. Conceptual diagram of clock and carrier synchronized multi-band wireless communications with optical frequency comb. PD: photodetector; BFP: bandpass filter; LPF: lowpass filter; PLL: phase-locked-loop; Tx: transmitter; Rx: receiver. The upper and lower branch illustrate the scenarios where kf_s tone is selected respectively, which is then used to up-convert baseband signal generated by DAC. The LPF filter at middle branch selects fs tone, which is used 1) as reference clock for DAC 2) for synchronous wireless clock distribution.

a potentially higher spectral efficiency (e.g. using high order formats) due to the higher signal-to-noise ratio (SNR) of DACs and ADCs. However, to cover multiple wireless frequency bands, multiple RF tones are needed for up-conversion, which adds cost and power consumption. Besides, even if the RF tones are phase-locked to the same reference oscillator within on RU, their high frequency (e.g. $\geq$10kHz) phase noise is often not coherent due to the limited input locking bandwidth (BW). As a result, short term (or high frequency) phase noise of different RF bands becomes uncorrelated, degrading the SNR of frequency-synthesized signals [19]. The un-correlated phase noise also affects performance of beam-forming in multiple-antenna radar system [20]. Additionally, RF tones at different RUs must be frequency synchronised to eliminate inter-channel crosstalk between frequency bands [6], [5]. Therefore, techniques to achieve RF carrier synchronization with high phase coherence are required in future radio access network.

Finally, distributing a low timing jitter synchronised clock is essential for applications requiring high accuracy positioning in future radio access network [11]. For example, in an trilateration positioning system [21], the positioning error is proportional to the timing error. Clock frequency synchronization, such as synchronous ethernet (Sync-E), is used in conjunction with precision time protocol (PTP) [22] to achieve precisely synchronized clock frequency and time [23]. Nevertheless, Synch-E only permits a precision of about ±10ns due to the relatively high frequency wander in the clock recovery modules, making it unable to support future applications that demand sub-nanosecond accuracy [24], [12]. Alternatively, previous studies proposed distributing clock signal to improve time synchronization accuracy significantly, with a proof-of-concept demonstration using wavelength division multiplexing (WDM) over optical fiber [12], [25]. Indeed, such a method has been proven effective in wired networks. It is, therefore, natural to investigate its feasibility in wireless systems, which motivated the transmission of clock signals in this work. that it has not been shown in wireless systems. A low jitter clock synchronization system would benefit wireless sensor networks, sensor localization and data aggregation applications [8], [9].

Previously we reported a system design to achieve simultaneous synchronization of clock and RF carriers by disseminating a filtered optical frequency comb through RoF links [26], [27]. However, in the preliminary demonstration, the clock was transmitted from the DU transmitter (Tx) to the wireless receiver (Rx) using coaxial cable, and only one RF band at 25 GHz was employed, which does not demonstrate the capability of synchronous clock distribution over wireless link and multiple frequency bands wireless transmission. To investigate the full system performance of the proposed clock and carrier synchronization technique, we improved the system design and implementation, including the frequency comb, carrier synchronization subsystem, wireless clock and data transmission systems, allowing us to demonstrate simultaneous wireless synchronous clock distribution and multiple bands wireless transmission. Specifically, we transmit a wireless clock through a 6.25 GHz carrier generated from the optical frequency comb, which is clock synchronized to the three RF carriers (12.5, 25 and 37.5 GHz) used for data transmission. The noise characterization and data transmission results validate the quality of the carriers and show the optimum design of their respectively RF signal chains. In addition, we theoretically model the impact of fibre chromatic dispersion on RF carrier power, which ultimately determines the signal quality in thermal noise limit electronic systems. Based on this model, we propose a comb power shaping method to minimize the RF power fading after transmission. Further, we experimentally investigate the RF carrier phase noise frequency scaling effect at both back-to-back and after fibre transmission, providing experiment base for the analysis of phase noise de-correlation.

II. Proof-of-Concept Experiment for Clock and Carrier Synchronized Wireless Communication Using Optical Frequency Comb

A. System architecture

The architecture of the envisaged clock and carrier synchronized wireless communication is shown in Fig. 1. At the DU

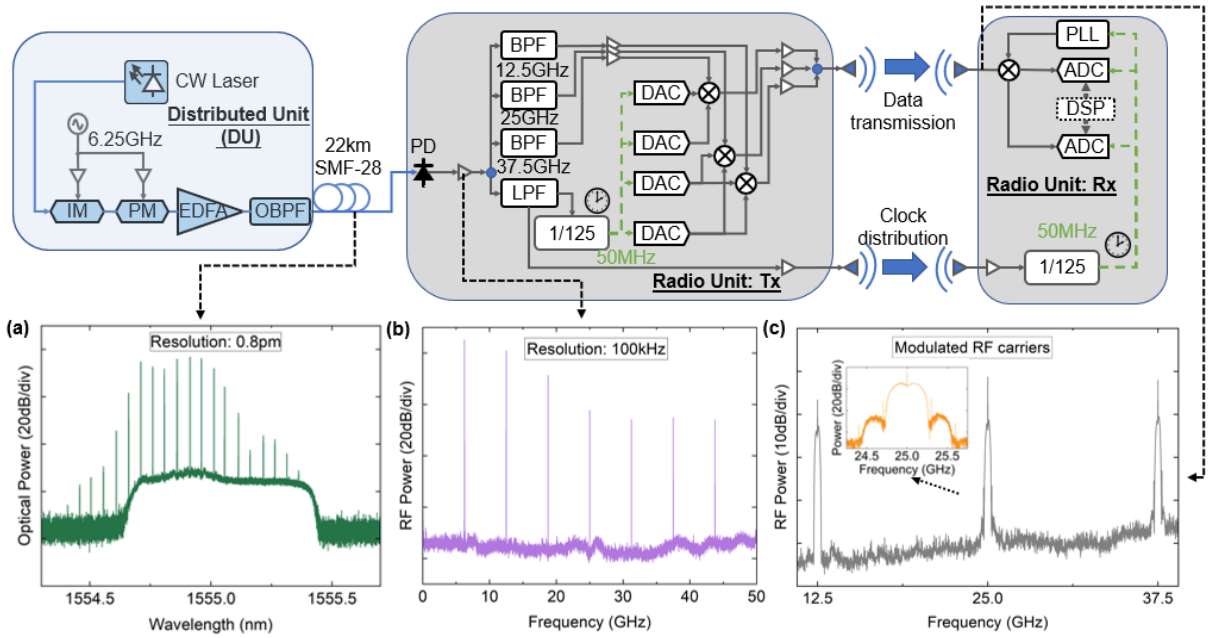

Fig. 2. Experimental setup. (a) Spectrum of optical frequency comb; (b) Spectrum of RF frequency comb; (c) RF spectrum of simultaneous transmission of 300MSymbol/s QPSK at 12.5, 25 and 37.5 GHz

side, an optical frequency comb with a channel spacing of f_s is distributed to different RUs through optical fiber. At wireless Tx side, a photodetector converts the comb signal to an RF frequency comb with a frequency spacing of f_s. Subsequently, the carrier frequency at f_s is filtered out and sent over the air for clock frequency synchronization. In practice, multiple divided harmonics of this RF signal can be used to minimize the impact of channel fading at a single frequency. The high order RF carriers, which are phase coherent to the clock signal, are filtered out as phase coherent carriers for signal modulation at different bands, which in principle can be used to create gap-less RF super-channel signal or providing access to white space frequencies for sensing and communications. At wireless receiver side, the distributed wireless clock is detected by antenna, which is used as reference clock for phase-locked-loop (PLL) for local oscillator generation. The wireless data centred at kf_s is down-converted to baseband by mixing with local oscillator.

Compared to previous studies using optical frequency comb to generate RF frequency comb [16], [17], [18], optical frequency comb in this work is generated through electro-optic modulation instead of using mode-locked laser (MLL), which provides superior RF carrier phase noise performance because phase noise of individual comb lines is fundamentally determined by RF driving signal phase noise and seed laser phase noise [28]. Additionally, the channel spacing of generated RF frequency comb can be easily tuned by changing RF driving signal frequency. Finally, it has to be mentioned that previous work only investigates the wireless transmission performance and impact of chromatic dispersion on first RF comb line [16], [17], [18], while our work further explores this idea by simultaneous demonstrating synchronized clock and RF carriers' distribution over multiple frequency bands.

B. Proof-of-concept experiment

Fig. 2 shows the proof-of-concept experimental setup consisting of a frequency comb source at central unit, which is transmitted to an RU via a 22 km standard single mode fiber (SSMF). In this proof-of-concept experiment, we only consider optical frequency comb is distributed to wireless transmitter while wireless receiver does not have optical fibre connection with DU (e.g. WLAN and wireless sensor network). The optical frequency comb is generated by modulating a 100-Hz linewidth 10-dBm power continuous wave (CW) laser using an optoelectronic (OE) frequency comb generating comprising an intensity modulator (IM) and a phase modulator (PM), both driven with a low-noise 6.25 GHz RF signal [26], [27]. The ultra-narrow linewidth laser and low-noise RF signal source together ensure strong coherence between the comb tones and is the key to generate low noise RF carriers after SSMF transmission. The EO comb was amplified from 6dBm to around 18dBm through an erbium-doped fiber amplifier (EDFA). A tunable optical bandpass filter with around 30GHz bandwidth is applied to attenuate right half of the optical frequency comb (see Fig. 2a). The purpose of optical filter is to introduce power difference among all comb lines and therefore significantly mitigate significantly the chromatic-dispersion-induced power fading of RF frequency comb, which crucial for power-stable and coherent RF carrier distribution [26]. The impact of chromatic dispersion on individual RF comb line power will be further investigated in detail in Section 4. After transmission, the optical frequency comb signals are detected by a 40-GHz photodetector (PD), yielding phase-coherent 6.25-GHz-spaced RF tones (RF frequency comb) through mixing between optical comb lines, which are subsequently amplified by a 40-GHz BW RF amplifier (see Fig. 2b).

Clock synchronization is achieved by extracting the first tone of RF frequency comb centered at 6.25 GHz using a 7-GHz BW low pass filter (LPF) then dividing down to 50 MHz using a programmable frequency divider (division ratio of 1/125), which is used as the reference clock the transmitter DAC for modulation signal generation. The extracted single tone 6.25 GHz RF signal is also amplified and sent to a dipole antenna (ANT-W63-WRT-SMA) for wireless clock broadcast. The 6.25GHz tone is not modulated, leading to minimized spectrum occupancies. Given such small bandwidth, the clock tone can co-exist with broadband signals. Since a single frequency signal was transmitted, narrow-band high-gain dipole antenna can be used to further improve power efficiency and reduce implementation cost.

Three RF carriers at 12.5, 25 and 37.5 GHz are extracted from RF frequency comb for multi-band wireless data transmission by using three bandpass filters centered at these frequencies. We only demonstrated three bands because of the availability of the RF components. In practice, any of the 6.25-GHz-spaced RF tones can be used for data transmission. However, the generated RF tone frequency is fundamentally determined by harmonics of the drive signal. To cover multiple high frequency channels with narrow spacing, a wideband narrow-spaced optical frequency comb is required. One possible solution is to generate densely spaced optical frequency comb, for example in [18] researchers using 1 GHz comb signal to generate RF carriers ranging from 1 to 140 GHz, which can be modulated with 1GHz bandwidth signals to populate the wireless spectrum.

The selected RF carriers are amplified to 14 dBm as LO and then modulated by four high resolution (16-bit) DACs to generate IQ modulated RF signals with up to 300 MSymbol/s using root-raise-cosine shaped (0.8 roll-off factor) QPSK and 16QAM formats. Due to the available number of DACs, the 12.5 GHz and 25 GHz carriers were modulated by the same DACs. The outputs of three IQ mixers were amplified separately before being combined and transmitted over the air using a wideband (6–53 GHz) 11-dBi gain quad-ridged horn antenna (SAV-0635331140).

The Rx quad-ridged horn antenna was placed in a direct line-of-sight in a cluttered indoor environment up to 4m away from the Tx. At the receiver side, a dipole antenna receives broadcast 6.25 GHz wireless clock signal, which is then fed into a frequency divider and outputs a 50 MHz synchronized reference clock signal. The reference clock is further split and used 1) to trigger analog-digital converter (ADC) and 2) as clock source for a phase-locked-loop (PLL), which generates the local oscillator (LO) for frequency down-conversion. Three frequency bands are tested individually by setting LO frequency to 12.5, 25, 37.5 GHz, respectively. After converting back to baseband, the in-phase and quadrature components of signal were captured by two ADCs followed by digital signal processing (DSP) for demodulation, including IQ imbalance compensation, match filtering and equalization. Advantageously, because of the synchronized carrier and clock, no carrier frequency synchronization and clock recovery are needed, which significantly reduces system complexity, DSP latency and power consumption. Fig. 2c shows the RF spectrum of the received signal, containing 300MSymobl/s QPSK signals centered around 12.5, 25 and 37.5 GHz. Due to lack of component, in this proof-of-concept experiment, the optical frequency comb is only distributed to transmitter RU for frequency up-conversion, while at receiver RU the LO for frequency down-conversion is generated by PLL, which potentially degrades phase noise performance. However, the optical comb can also be distributed to receiver RU for simplified and high performance down-conversion by using the same scheme as transmitter side.

III. Experimental Results

A. Phase noise of RF frequency comb

For wireless transmission system, the phase noise of RF carriers has a strong impact on signal quality due to phase rotations in the constellation [29]. The practicability and efficacy of this new method is illustrated through phase noise measurements of distributed RF carriers (as shown in Fig. 3). The solid line in Fig. 3 shows the phase noise of RF carriers after 22 km SSMF transmission, generated using our proposed scheme. Orange, blue and red curves correspond 12.5, 25 and 37.5GHz, respectively. The root-mean-square (rms) jitter (integrated from 1kHz to 10MHz) equals to 75, 73 and 59 fs for 12.5, 25 and 37.5GHz, respectively. The lower boundary of phase noise measurement is set to 1kHz, because the data capture time for later EVM measurement is relatively short (around $500\mu s$), thus the impact of low frequency phase noise is less dominant. When comparing the solid orange and blue curves, it can be observed that the phase noise of 25GHz tone is 6dB higher than 12.5GHz, which follows phase noise scaling of an ideal RF frequency multiplier, resulting in similar amount of integrated jitter. Note that the rms jitter of 37.5GHz tone is even lower than 12.5 and 25GHz tone. One possible reason is that there is fewer number of 37.5-GHz spaced optical tones pair in our optical frequency comb, resulting in a less significant impact from seed laser phase noise de-correlation. The impact of fiber chromatic dispersion and seed laser phase noise on generated RF carrier phase noise will be analyzed in the next section. Dashed lines in Fig. 3 shows the measured phase noise of a commercially available electronic phase locked loop (PLL) based RF oscillator (TI LMX2595). The results shows that our distributed RF carriers exhibit a significantly lower phase noise and integrated jitter values is nearly ten times better than the electronic PLL (about 760fs). The relatively higher phase noise in the high frequency offset region (1-10MHz) is due to the larger output PLL bandwidth of the used RF source at the RU, which can be further improved using dielectric resonant oscillators (DRO).

B. Clock and carrier synchronized wireless transmission

Fig. 4a and b show the measured error vector magnitude (EVM) for different received RF power for QPSK at 100 and 300 MSymbol/s at three frequency bands respectively. The solid line represented the electrical back-to-back transmission, in this case, the received RF power is adjusted by

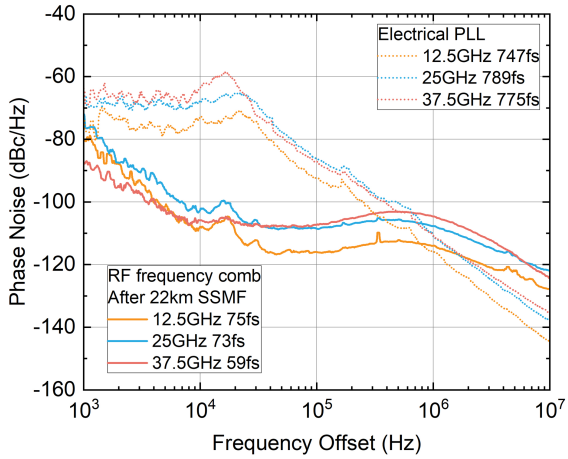

Fig. 3. Phase noise measurement of 12.5, 25 and 37.5GHz RF carrier generated using proposed scheme and commercial RF oscillator

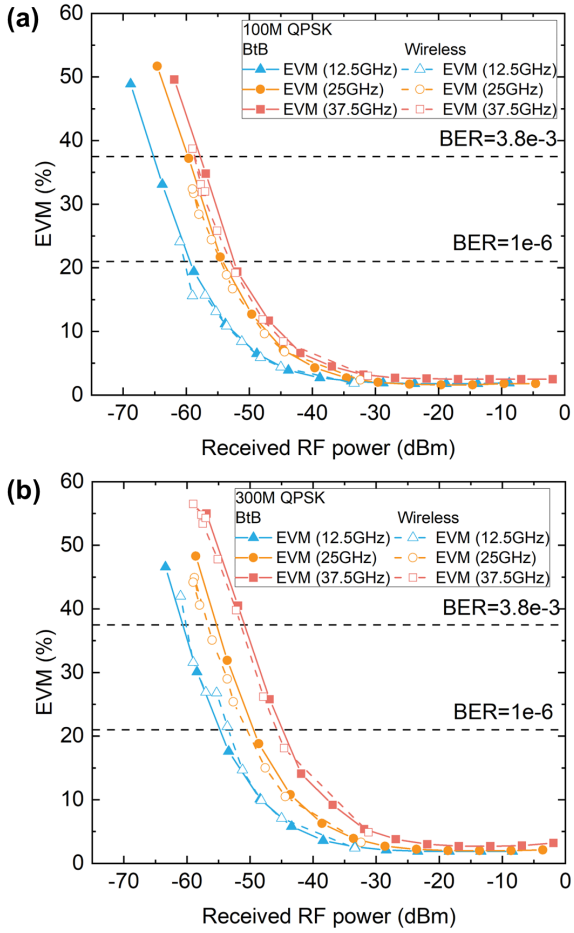

Fig. 4. EVM v. received RF power at BtB and wireless transmission for (a) 100 MSym/s QPSK and (b) 300 MSym/s QPSK.

adding attenuation at receiver side. The dashed line showed the wireless transmission results, when the distance between horn antenna increases from 0.4m to 4m, the received RF power is reduced from -33 to -54 dBm, which matches with the calculated free-space path loss. For 100 MSymbol/s QPSK, the measured back-to-back RX sensitivities at HD-FEC threshold (BER=3.8e-3, EVM=37.5%) for 12.5, 25 and 37.5 GHz channels are -63, -57 and -54 dBm, respectively. The better receiver sensitivity of 12.5 GHz is due to the better image rejection of the low-speed IQ-mixer used for this channel. The 25 GHz channel slightly outperforms 37.5 GHz even with lower modulation signal power (as we divided the DAC outputs to modulate 12.5 and 25 GHz carrier), this is because the IQ mixer used for this experiment 1) has about 5 dB higher IQ conversion loss at 37.5 GHz compared to 25 GHz and 2) the conversion loss gradually increases from 36 to 40 GHz, affecting the flatness of spectrum. Due to the limited transmission distance tested, we were not able to measure the HD-FEC RX sensitivity for 100 MSymbol/s QPSK wireless transmission. However, the rest of the curve matches with back-to-bac results, which suggests that our wireless transmission is limited by power rather than multi-path interference. When the baud rate increases from 100 to 300 MSymbol/s, the HD-FEC RX sensitivities after wireless transmission for three frequency channels are -59, -55 and -47 dBm, respectively. The sensitivity difference between 25 and 37.5 GHz is increased to from 3 to 8 dB because of the impact of non-uniform conversion loss becomes significantly as modulation bandwidth increases.

Fig. 5a and b show the measured EVM at different received RF power for 100 and 300 MSymbol/s 16QAM at electrical back-to-back and after wireless transmission. The HD-FEC (BER=3.8e-3, EVM=17.5%) RX sensitivities for 100 MSymbol/s 16QAM 12.5, 25, 37.5 GHz channels are -54, -50 and -48 dBm, respectively. Note that, compared to QPSK case, where in high received power region, all three channels exhibit similar performance, for 16QAM case, 12.5 GHz has the best performance among three because 1) a more linear RF amplifier is used to amplify RF carrier and 2) 16QAM modulation is more sensitive to non-linear distortion. When baud rate is increased to 300 MSymbol/s, the HD-FEC RX sensitivities become -50, -45 and -38 dBm, respectively, for the 12.5, 25 and 37.5 GHz bands.

Finally, as shown in Fig. 6, we evaluate the wireless transmission distance at the HD-FEC threshold and show a 300 MSymbol/s QPSK transmission distance of 4, 3 and 2 meters for 12.5, 25 and 37.5GHz bands, respectively. For 300 MSymbol/s 16QAM, the corresponding transmission distance is reduced 1.4, 1.2 and 0.8 meters, for 12.5, 25 and 37.5 GHz bands, respectively. All results were obtained using synchronized clock and carriers without carrier frequency recovery DSP.

IV. Impact of Chromatic Dispersion on RF Carrier Power and Phase Noise

A. Mitigating RF power fading after SSMF transmission

One of the key considerations of the purposed scheme is the RF carrier power variation with fiber transmission distance.

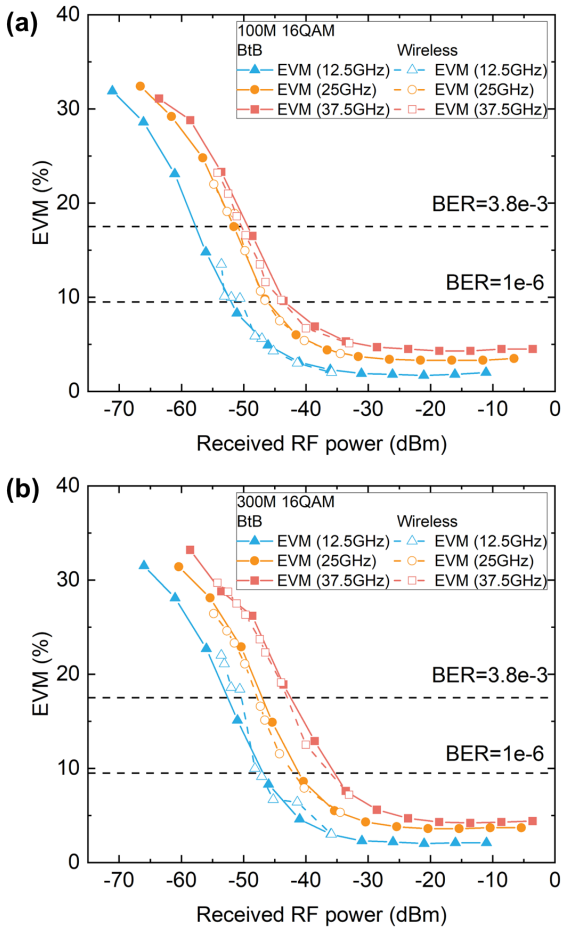

Fig. 5. EVM v. received RF power at BtB and wireless transmission for (a) 100 MSym/s 16QAM and (b) 300 MSym/s 16QAM.

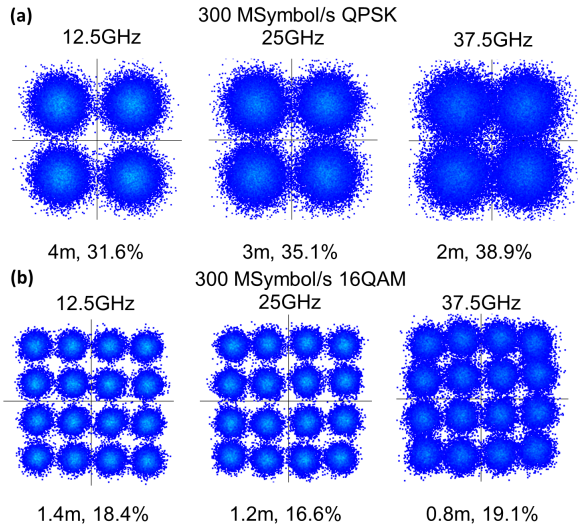

Fig. 6. Measured constellation diagrams for different bands at different wireless transmission distances.

The chromatic dispersion of optical fiber introduces phase shift to all optical frequency comb lines, leading to constructive or destructive interference of RF signal [18]. As a result, the power of distributed RF carrier might significantly drop at certain transmission distance. Previous studies have shown a simplified model characterizing such power fading effect and purpose using waveshaper to pre-compensate fiber dispersion [17], [30], however these studies only focus on the first RF frequency comb line and dispersion compensation needs to be calibrated for different transmission length. Another study experimentally measures RF frequency comb power at two different transmission distances, which does not provide the relationship between dispersion and power of high order RF comb lines. Here, we modelled the impact of chromatic dispersion on power of RF frequency comb. Based on this model, we further proposed and demonstrated using optical spectrum shaping to mitigate the power fading effect of RF frequency comb.

Considering a linear chirped optical frequency comb signal and dispersion slope is neglected due to the relatively small overall comb bandwidth in this study. After fiber transmission, the optical frequency comb is detected by a photodetector, converting received optical power to electric current, its output can be represented by:

$$I(t,n,L) = exp(-\alpha L)\cdot \left| \sum_{n=-N}^{N} A_n exp[j(2\pi(f_c + nf_m)t - \beta_2 2\pi^2 L(nf_m)^2 + \phi_0(t(n,L)) + n\phi_{rf}(t(n,L))]\right|^2 \quad (1)$$

α represents fiber attenuation, L stands for fiber length, n stands for the order of optical tone (here we define the center optical tone as n=0), A_n represents the amplitude of n^{th} optical tone, f_c stands for center optical frequency, f_m is the channel spacing of optical frequency comb, β_2 is the second-order dispersion coefficient. The phase noise of n^{th} line of electro-optic comb is the sum of ϕ_0 (the seed laser phase noise) and $n\phi_{rf}$ (RF driver phase noise) [28], [31] (i.e. $\phi_n = \phi_0 + n\phi_{rf}$). Note that phase noise coherence between comb lines depends on the group velocity delay, which is determined by the frequency offset between lines and chromatic dispersion of optical fiber, this is considered by the $t(n,L)$ in Equ. 1. The nth order of RF frequency comb is generated by summing up the beat tone of optical comb line with n times of channel spacing.

In our proof-of-concept experiment shown in previous section, the channel spacing of electro-optic comb is set to 6.25GHz and we demonstrated the wireless transmission at 12.5, 25 and 37.5GHz, which corresponds to second, fourth and sixth order RF comb line. To generate RF carrier at frequency at $6f_s$, at least 7 optical comb lines is needed (i.e. N = 3). Herein, we firstly analyzed the RF carrier power only, thus the phase noise terms in Equ. 1 are ignored for simplicity as these does not affect RF power. The RF carrier phase noise will be experimentally investigated later in this section. Based on Equ. 1, the expression for second, fourth and sixth order

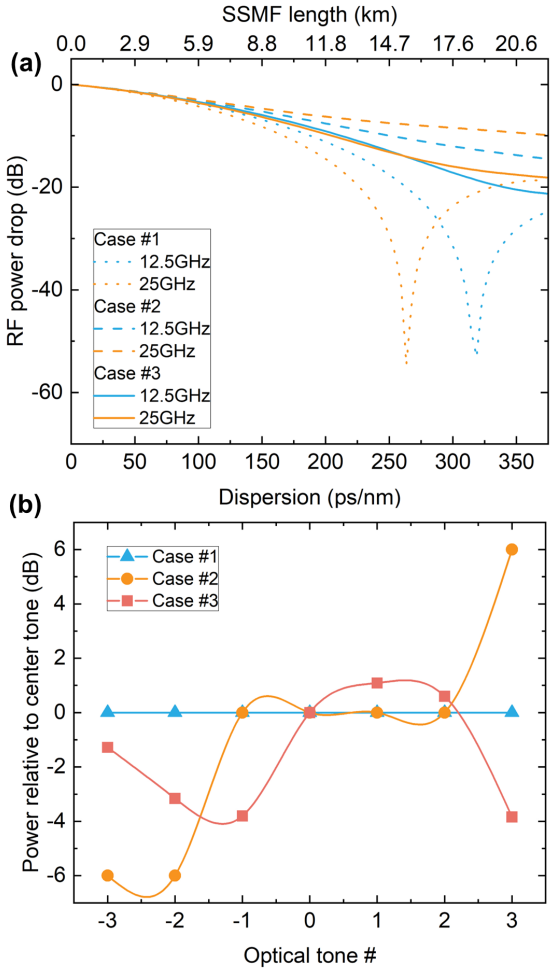

Fig. 7. (a) RF comb power drop with different transmission distance and (b) Optical comb power coefficient for three different spectrum shaping profiles

of RF frequency comb can be expressed as follows:

$$P_2(t,n,L) = 2exp(-\alpha L)\cdot [A_0A_2cos(4\pi f_m t - 8\beta_2\pi^2 L f_m^2) + A_0A_{-2}cos(4\pi f_m t + 8\beta_2\pi^2 L f_m^2) + A_1A_{-1}cos(4\pi f_m t) + A_1A_3cos(4\pi f_m t - 16\beta_2\pi^2 L f_m^2) + A_{-1}A_{-3}cos(4\pi f_m t + 16\beta_2\pi^2 L f_m^2)] \quad (2)$$

$$P_4(t,n,L) = 2exp(-\alpha L)\cdot [A_{-1}A_3cos(8\pi f_m t - 16\beta_2\pi^2 L f_m^2) + A_1A_{-3}cos(8\pi f_m t + 16\beta_2\pi^2 L f_m^2) + A_2A_{-2}cos(8\pi f_m t)] \quad (3)$$

$$P_6(t,n,L) = 2exp(-\alpha L)\cdot A_{-3}A_3cos(12\pi f_m t) \quad (4)$$

Taking second order RF comb as an example (i.e. Equ. 2), if $A_2 = A_{-2}$, the summation of first and second term inside bracket equals to $cos(4f_m t)cos(8\beta_2\pi^2 L f_m^2)$ and similarly if $A_1A3 = A_{-1}A_{-3}$, the summation of fourth and fifth term inside bracket equals to $cos(4f_m t)cos(16\beta_2\pi^2 L f_m^2)$. If the amplitude coefficients of all terms inside the bracket are the same, the power of second order RF comb is modulated by $1 + cos(8\beta_2\pi^2 L f_m^2) + cos(16\beta_2\pi^2 L f_m^2)$. Similarly, for the fourth order RF comb, its power will be modulated by $1 + cos(16\beta_2\pi^2 L f_m^2)$. As a result, this leads to power fading after fiber transmission. Note that for 6^{th} order RF comb, its power is not affected by dispersion, as it is generated solely by the beating between $+3^{rd}$ and -3^{rd} tone of optical tone. On the other hand, if we shape the optical spectrum so that the amplitude of one of the beat tone is dominant, the impact of chromatic dispersion can potentially be suppressed as it only introduce additional phase change rather changing its power.

Based on this concept, we vary the power of each optical comb line and models its impact on the RF frequency comb power. In this case, we set the channel spacing to 6.25GHz (same as in experiment), the number of optical frequency comb line is set to 7, and only focusing on second and fourth order (as the power of sixth order is independent of fiber dispersion). The SSMF fiber length is swept from 0 to 22km (match with experiment) and dispersion coefficient is set to 17ps/km/nm. To illustrate the impact of different spectrum profile on RF tone power after fiber transmission, three cases are studied (as shown in Fig. 7b). For Case #1, all optical comb lines have even power, for Case #2, power of each line is optimized to minimize power fading and for Case #3, we use measured value from proof-of-concept experiment, only the center 7 tones are considered as the power of rest of comb lines are more than 10dB lower than center tone. Fig. 7a shows the 12.5 and 25GHz RF carrier power drop after transmission. For Case #1 (shown by dotted line), power fading occurs after 15km and 18km fiber transmission for 12.5 and 25GHz, respectively. This is caused by the dispersion induced amplitude modulation described earlier. For Case #2 (dashed line), the power fading is eliminated and both RF carriers power remains flat across the testing range, with around 10dB power drop compared to BtB case, which is mainly due to the fiber attenuation. Finally for Case #3 (solid line), power fading does not occur within 22km for both RF carriers and power gradually drops as transmission distance increases. However, compared to Case #2, the power drop at 22km are higher (18dB compared to 10dB), this is attributed to the limited roll-off and bandwidth of the optical bandpass filter we used in this experiment. The RF carrier power flatness can be improved by adjusting the driving voltage of both IM and PM or fine tune the bias voltage of IM to control the power of each optical comb line. Alternatively, one can use waveshaper to program the power of each optical comb line. Nevertheless, the results shown in Fig. 7 have proven the purposed solution provides a simple and cost-effective way to eliminate power fading and improve the RF carrier power flatness after fiber transmission, which is crucial for multi-band wireless communication using RF frequency comb.

B. RF carrier phase noise penalty after SSMF transmission

To further investigate the determinate factors of generated RF carrier phase noise, we experimentally measured the phase noise of the whole RF frequency comb after various fiber transmission distances with seed lasers with different linewidth. For this specific measurement, the optical frequency comb channel spacing is set to 5GHz. The measurement range of

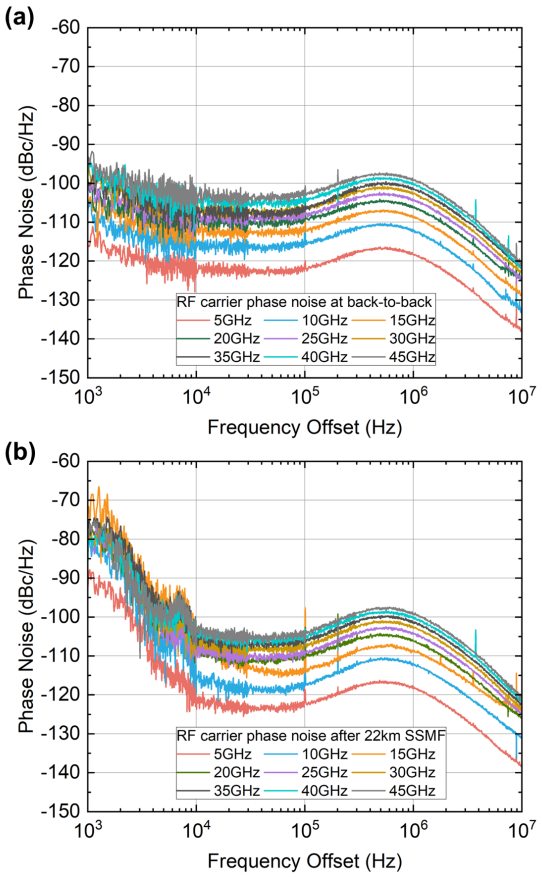

Fig. 8. Phase noise of 5-45GHz RF carrier generated using proposed scheme at (a) optical back-to-back and (b) after 22km SSMF transmission

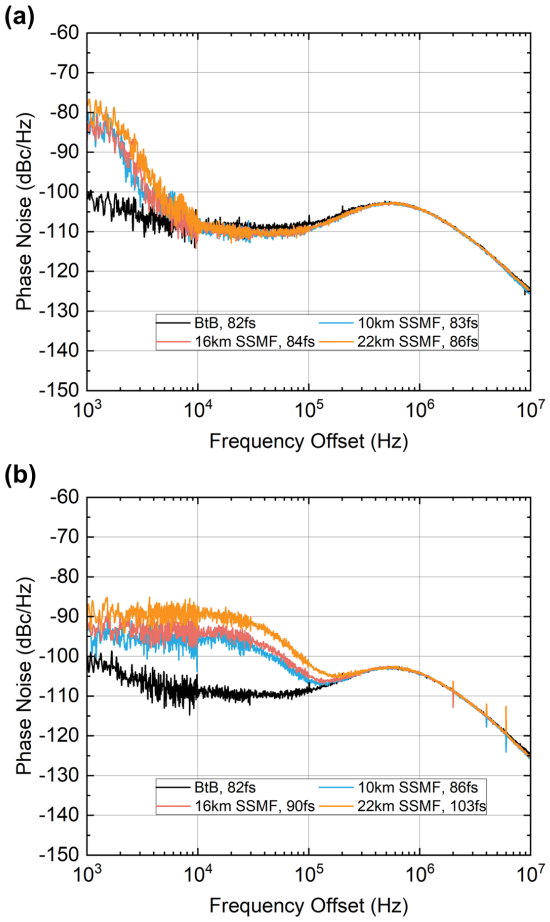

Fig. 9. Phase noise 25GHz RF carrier generated using proposed scheme with (a) 100-Hz linewidth seed laser and (b) 100-kHz linewidth seed laser

phase noise analyzer is up to 50GHz, 5GHz channel spacing results up to 10 5-GHz spaced RF carriers from 5-50GHz, which can potentially provide a more detailed insight on phase noise scaling compared to wider channel spacing (i.e. 6.25GHz used in wireless transmission demonstration). Fig. 8a and b compare the phase noise of 5-45GHz RF carriers at optical back-to-back and after 22km SSMF transmission. In this case, 100-Hz linewidth seed laser is used. For back-to-back case, the phase noise scales by around 20log(N) when carrier frequency is multiplied by N, which is identical to a RF oscillator. The integrated rms jitter is around 85fs for all RF carriers, suggesting the proposed RF carrier generation scheme does not cause any phase noise performance degradation [32]. This result can be justified by Equ. 1. When L equals to 0, all comb lines arrive at photodetector at the same time, which means seed laser and RF driver phase noise remains correlated. Thus the beat tone phase noise equals to the subtraction of phase noise of two optical comb lines. Compared to back-to-back case, the high frequency region (from 10kHz to 10MHz) of RF carrier phase noise remains similar after 22km SSMF transmission, where the low frequency phase noise (from 1kHz to 10kHz) is degraded. This is because the chromatic dispersion of SSMF introduces group velocity difference to optical tones and consequently, leading to enhanced phase noise in the low frequency region. Note that the degraded phase noise is primarily in the low frequency region, the low frequency flicker and random walk should be attributed to the increased jitter [26].

Finally, Fig. 9 compares the 25GHz RF carrier phase noise after different SSMF transmission distances. The 25GHz RF carrier is generated based on seed laser with 100-Hz linewidth (Fig. 9a) and 100-kHz linewidth (Fig. 9b). As expected, the phase noise becomes more de-correlated as transmission distance increases, increasing to an increased rms jitter from 82fs to 86fs for 100-Hz seed laser and from 82fs to 103fs for 100-kHz seed laser, respectively [33]. Note that at optical back-to-back, the phase noise exhibits very similar performance for both seed lasers, indicating seed laser phase noise does not contribute to RF carrier phase noise. Because the seed laser phase noise of two comb lines is completely cancelled out after beating. However, when a low linewidth laser, the phase noise degradation after fiber transmission is less significant, with only the low frequency phase noise (1kHz to 10kHz) increases. With 100-kHz linewidth laser as seed, the phase noise from 1kHz to 100kHz increases significantly. These results indicate that with low phase noise seed laser, the generated RF carrier phase noise degradation caused by phase noise de-correlation can be minimized, ensuring low phase noise RF carrier distribution over longer transmission distance.

V. Conclusion

We have demonstrated the simultaneous distribution of low phase noise frequency synchronized clock and 6.25-GHz spaced RF carriers using the electro-optic frequency comb technique. With the proposed scheme, we have demonstrated synchronous multi-band 1.2 Gb/s wireless transmission at 12.5, 25 and 37.5GHz over 3-meter distance over the air. The proposed method is shown to achieve 1) low timing jitter wireless clock distribution and 2) low phase noise carrier distribution between DUs and RUs, ultimately enabling low latency and high-capacity fibre-wireless transmission. A mathematical model is developed to characterize and optimize the power of the RF carrier (generated through frequency comb line beating) after SSMF transmission. Based on this model, we demonstrated that RF power fading introduced by fiber chromatic dispersion can be potentially mitigated by optimizing the frequency comb power envelope, enabling stable power RF carrier distribution over long distances. Finally, our results show that the chromatic dispersion of the fiber causes laser phase noise de-correlation, leading to RF carrier phase noise penalty after transmission. With a low linewidth laser as the seed for the electro-optic comb, the penalty can be minimized, ensuring low phase noise carrier distribution.

References

[1] J. Kim, M. Sung, S.-H. Cho, Y.-J. Won, B.-C. Lim, S.-Y. Pyun, J.-K. Lee, and J. H. Lee, "Mimo-supporting radio-over-fiber system and its application in mmwave-based indoor 5g mobile network," *Journal of Lightwave Technology*, vol. 38, no. 1, pp. 101–111, 2020.

[2] E.-S. Kim, M. Sung, J. H. Lee, J. K. Lee, S.-H. Cho, and J. Kim, "Coverage extension of indoor 5g network using rof-based distributed antenna system," *IEEE Access*, vol. 8, pp. 194 992–194 999, 2020.

[3] A. N. Uwaechia and N. M. Mahyuddin, "A comprehensive survey on millimeter wave communications for fifth-generation wireless networks: Feasibility and challenges," *IEEE Access*, vol. 8, pp. 62 367–62 414, 2020.

[4] X. Pang, O. Ozolins, S. Jia, L. Zhang, R. Schatz, A. Udalcovs, V. Bobrovs, H. Hu, T. Morioka, Y.-T. Sun, J. Chen, S. Lourdudoss, L. K. Oxenløwe, S. Popov, and X. Yu, "Bridging the terahertz gap: Photonics-assisted free-space communications from the submillimeter-wave to the mid-infrared," *Journal of Lightwave Technology*, vol. 40, no. 10, pp. 3149–3162, 2022.

[5] N. Argyris, G. Giannoulis, K. Kanta, N. Iliadis, C. Vagionas, S. Papaioannou, G. Kalfas, D. Apostolopoulos, C. Caillaud, H. Debrégeas, N. Pleros, and H. Avramopoulos, "A 5g mmwave fiber-wireless ifof analog mobile fronthaul link with up to 24-gb/s multiband wireless capacity," *Journal of Lightwave Technology*, vol. 37, no. 12, pp. 2883–2891, 2019.

[6] A. Bekkali, S. Ishimura, K. Tanaka, K. Nishimura, and M. Suzuki, "Multi-if-over-fiber system with adaptive frequency transmit diversity for high capacity mobile fronthaul," *Journal of Lightwave Technology*, vol. 37, no. 19, pp. 4957–4966, 2019.

[7] Ericsson and Deutsche Telekom, *Enabling time-critical applications over 5G with rate adaptation (white paper)*. Ericsson and Deutsche Telekom, 2021.

[8] A. Dongare, P. Lazik, N. Rajagopal, and A. Rowe, "Pulsar: A wireless propagation-aware clock synchronization platform," in *2017 IEEE Real-Time and Embedded Technology and Applications Symposium (RTAS)*, 2017, pp. 283–292.

[9] A. Mahmood, R. Exel, H. Trsek, and T. Sauter, "Clock synchronization over ieee 802.11—a survey of methodologies and protocols," *IEEE Transactions on Industrial Informatics*, vol. 13, no. 2, pp. 907–922, 2017.

[10] H. Cho, J. Jung, B. Cho, Y. Jin, S.-W. Lee, and Y. Baek, "Precision time synchronization using ieee 1588 for wireless sensor networks," in *2009 International Conference on Computational Science and Engineering*, vol. 2, 2009, pp. 579–586.

[11] Z. Zhou, J. Wei, Y. Luo, K. A. Clark, E. Sillekens, C. Deakin, R. Sohanpal, R. Slavík, and Z. Liu, "Communications with guaranteed bandwidth and low latency using frequency-referenced multiplexing," *Nature Electronics*, vol. 6, no. 9, pp. 694–702, 2023.

[12] K. A. Clark, Z. Zhou, and Z. Liu, "Clock synchronizing radio access networks to picosecond precision using optical clock distribution and clock phase caching," *J. Opt. Commun. Netw.*, vol. 16, no. 1, pp. A89–A97, Jan 2024. [Online]. Available: https://opg.optica.org/jocn/abstract.cfm?URI=jocn-16-1-A89

[13] J. Beas, G. Castanon, I. Aldaya, A. Aragon-Zavala, and G. Campuzano, "Millimeter-wave frequency radio over fiber systems: A survey," *IEEE Communications Surveys and Tutorials*, vol. 15, no. 4, pp. 1593–1619, 2013.

[14] C. Lim, Y. Tian, C. Ranaweera, T. A. Nirmalathas, E. Wong, and K.-L. Lee, "Evolution of radio-over-fiber technology," *Journal of Lightwave Technology*, vol. 37, no. 6, pp. 1647–1656, 2019.

[15] T. Bo, H. Kim, Z. Tan, and Y. Dong, "Optical single-sideband transmitters," *Journal of Lightwave Technology*, vol. 41, no. 4, pp. 1163–1174, 2023.

[16] F. Brendel, J. Poette, B. Cabon, T. Zwick, F. van Dijk, F. Lelarge, and A. Accard, "Chromatic dispersion in 60 ghz radio-over-fiber networks based on mode-locked lasers," *Journal of Lightwave Technology*, vol. 29, no. 24, pp. 3810–3816, 2011.

[17] H. H. Elwan, J. Poette, and B. Cabon, "Simplified chromatic dispersion model applied to ultrawide optical spectra for 60 ghz radio-over-fiber systems," *Journal of Lightwave Technology*, vol. 37, no. 19, pp. 5115–5121, 2019.

[18] H. Boerma, F. Ganzer, P. Runge, M. Schell, E. Fernandes, B. Rudin, and F. Emaury, "Microwave photonic ps-pulse and 140ghz rf comb generator," *Journal of Lightwave Technology*, pp. 1–6, 2023.

[19] X. Yi, N. K. Fontaine, R. P. Scott, and S. J. B. Yoo, "Tb/s coherent optical ofdm systems enabled by optical frequency combs," *Journal of Lightwave Technology*, vol. 28, no. 14, pp. 2054–2061, 2010.

[20] K. Siddiq, M. K. Hobden, S. R. Pennock, and R. J. Watson, "Phase noise in fmcw radar systems," *IEEE Transactions on Aerospace and Electronic Systems*, vol. 55, no. 1, pp. 70–81, 2019.

[21] B. Jaduszliwer and J. Camparo, "Past, present and future of atomic clocks for gnss," *GPS Solutions*, vol. 25, no. 1, p. 27, Jan 2021. [Online]. Available: https://doi.org/10.1007/s10291-020-01059-x

[22] IEEE, "Ieee standard for a precision clock synchronization protocol for networked measurement and control systems," *IEEE Std 1588-2008 (Revision of IEEE Std 1588-2002)*, pp. 1–269, 2008.

[23] M. Lipiński, T. Włostowski, J. Serrano, and P. Alvarez, "White rabbit: A PTP application for robust sub-nanosecond synchronization," *IEEE International Symposium on Precision Clock Synchronization for Measurement, Control, and Communication, ISPCS*, pp. 25–30, 2011.

[24] K. A. Clark, D. Cletheroe, T. Gerard, I. Haller, K. Jozwik, K. Shi, B. Thomsen, H. Williams, G. Zervas, H. Ballani, P. Bayvel, P. Costa, and Z. Liu, "Synchronous subnanosecond clock and data recovery for optically switched data centres using clock phase caching," *Nature Electronics*, vol. 3, pp. 426–433, 7 2020.

[25] P. T. Dat, A. Kanno, N. Yamamoto, and T. Kawanishi, "Full-duplex transmission of lte-a carrier aggregation signal over a bidirectional seamless fiber-millimeter-wave system," *Journal of Lightwave Technology*, vol. 34, no. 2, pp. 691–700, 2016.

[26] Z. Zhou, D. Nopchinda, M.-C. Lo, I. Darwazeh, and Z. Liu, "Simultaneous clock and rf carrier distribution for beyond 5g networks using optical frequency comb," in *2022 European Conference on Optical Communication (ECOC)*, 2022, pp. 1–4.

[27] D. Nopchinda, Z. Zhou, Z. Liu, and I. Darwazeh, "Multiband comb-enabled mm-wave transmission," *IEEE Transactions on Microwave Theory and Techniques*, vol. 72, no. 1, pp. 787–796, 2024.

[28] C. Deakin, Z. Zhou, and Z. Liu, "Phase noise of electro-optic dual frequency combs," *Opt. Lett.*, vol. 46, no. 6, pp. 1345–1348, Mar 2021. [Online]. Available: https://opg.optica.org/ol/abstract.cfm?URI=ol-46-6-1345

[29] J. Chen, D. Kuylenstierna, S. E. Gunnarsson, Z. S. He, T. Eriksson, T. Swahn, and H. Zirath, "Influence of white lo noise on wideband communication," *IEEE Transactions on Microwave Theory and Techniques*, vol. 66, no. 7, pp. 3349–3359, 2018.

[30] H. H. Elwan, C. Browning, J. Poette, L. P. Barry, and B. Cabon, "Compensation of fiber dispersion induced-power fading in reconfigurable millimeter-wave optical networks," *Optics Communications*, vol. 476, p. 126308, 2020. [Online]. Available: https://www.sciencedirect.com/science/article/pii/S0030401820307252

[31] V. Torres-Company and A. M. Weiner, "Optical frequency comb technology for ultra-broadband radio-frequency photonics," *Laser &*

Photonics Reviews, vol. 8, no. 3, pp. 368–393, 2014. [Online]. Available: https://onlinelibrary.wiley.com/doi/abs/10.1002/lpor.201300126

[32] E. S. Lima, N. Andriolli, E. Conforti, G. Contestabile, and A. Cerqueira Sodré, "Low-phase-noise tenfold frequency multiplication based on integrated optical frequency combs," *IEEE Photonics Technology Letters*, vol. 34, no. 16, pp. 878–881, 2022.

[33] Z. Zhou, K. A. Clark, C. Deakin, and Z. Liu, "Clock synchronized transmission of 51.2 gbd optical packets for optically switched data center interconnects," *J. Lightwave Technol.*, vol. 40, no. 6, pp. 1735–1741, Mar 2022. [Online]. Available: https://opg.optica.org/jlt/abstract.cfm?URI=jlt-40-6-1735

Zichuan Zhou (Member, IEEE) received the B.Eng. degree in electronic and electrical engineering from University College London, London, U.K., in 2018, the M.Res. degree in integrated photonic and electronic systems from the University of Cambridge, Cambridge, U.K., in 2019 and Ph.D degree in electronic and electrical engineering from University College London, London, U.K., in 2024. His research interests include data center interconnects, radio access networks, passive optical networks, optical frequency comb applications, and low-latency optical transceivers.

Dhecha Nopchinda (Member, IEEE) was born in Bangkok, Thailand, in 1991. He received the B.Eng. degree (First Class Hons.) in electronic and communication engineering from the Sirindhorn International Institute of Technology, Thammasat University, Thailand, in 2013, the M.Sc. degree (with distinction) in wireless and optical communication from the University College London, U.K., in 2014, and the Ph.D. degree in microtechnology and nanoscience from Chalmers University of Technology, Gothenburg, Sweden, in 2019.

From 2015 to 2020, he was with the Microwave Electronics Laboratory at Chalmers University of Technology. Funded by the Leverhulme Trust's Early Career Fellowship, he was with the Department of Electronic and Electrical Engineering at University College London from 2020 to 2023, where he helped setup and managed the mm-wave laboratory and led the mm-wave measurement research work. In 2023, he joined Gotmic, a mm-wave circuit and system design house in Gothenburg, Sweden, as a microwave system engineer, where he currently leads the system-level measurements and characterization workgroup. His research interests include digital techniques and signal processing for experimental high data-rate communication and mm-wave instrumentation.

Dr. Nopchinda was the recipient of a scholarship to study at the Sirindhorn International Institute of Technology from 2009 to 2013, the Leverhulme Trust's Early Career Fellowship from 2020 to 2023, and the inaugural First Place in IEEE Microwave Theory and Technology Society's Early Career Paper Competition at the 2023 International Microwave Symposium.

Izzat Darwazeh (Senior Member, IEEE) received the Graduate degree in electrical engineering from the University of Jordan, Amman, Jordan, in 1984, and the M.Sc. and Ph.D. degrees from the University of Manchester, Manchester, U.K., in 1986 and 1991, respectively.

He holds the University of London Chair of communications engineering and leads the 70-Strong Information and Communications Engineering Group, Department of Electronic and Electrical Engineering, University College London, London, U.K., where he is also the Director of the Institute of Communications and Connected Systems. He has authored/co-authored more than 250 papers and book chapters in the areas of optical and wireless communications and monolithic microwave integrated circuits and high-speed/frequency circuits. He coedited Analogue Optical Fibre Communications (IEE, 1995) and Newness Book on Electrical Engineering (Elsevier) in 2008. He has also co-authored two books Linear Circuit Analysis and Modeling (Elsevier in 2005) and Microwave Active Circuit Analysis and Design (Academic Press, in 2015). In 2002, he proposed (with Miguel Rodrigues) the Fast OFDM concept and in 2003 the SEFDM concept and has been working on these topics since. He currently teaches mobile and wireless communications and circuit design and his current research activities are in ultra high-speed microwave circuits and in wireless and optical communication systems.

Dr. Darwazeh is a Chartered Engineer and a Fellow of IET and the Institute of Telecommunications Professionals.

Zhixin Liu (Senior Member, IEEE) received the B.Eng. degree in information engineering and the B.B.A. degree in business administration from Tianjin University, Tianjin, China, in 2006, the M.S. degree in electrical engineering from Shanghai Jiao Tong University, Shanghai, China, in 2009, and the Ph.D. degree in information engineering from the Chinese University of Hong Kong, Hong Kong, in 2012.

In 2013, he joined the Optoelectronics Research Centre, University of Southampton, Southampton, U.K. In 2016, he joined the Department of Electronics and Electrical Engineering, University College London, London, U.K. His research focuses on exploring analog and optical signal processing techniques for high performance communication systems, including high-speed direct modulation, frequency comb, photonic-assisted data conversion, and low-latency data communications.

Dr. Liu is a Senior Member of Optica.